Sensors and Actuators B 238 (2017) 1052–1059

Contents lists available at ScienceDirect

Sensors and Actuators B: Chemical

journal homepage: www.elsevier.com/locate/snb

Controllable synthesis of Co_3O_4 crossed nanosheet arrays toward an acetone gas sensor

Ziyue Zhang [a], Liping Zhu [a,*], Zhen Wen [a,b], Zhizhen Ye [a]

[a] State Key Laboratory of Silicon Materials, School of Materials Science and Engineering, Cyrus Tang Center for Sensor Materials and Applications, Zhejiang University, Hangzhou, 310027, China
[b] Institute of Functional Nano and Soft Materials (FUNSOM), Soochow University, Suzhou, Jiangsu, 215123, China

ARTICLE INFO

Article history:
Received 14 March 2016
Received in revised form 22 July 2016
Accepted 26 July 2016
Available online 27 July 2016

Keywords:
Cobalt oxide
Crossed nanosheet arrays
Gas sensor
Low temperature

ABSTRACT

Co_3O_4 crossed nanosheet (CNS) arrays were successfully synthesized by a post-thermal conversion of $(Co(NH_3)_6)CoF_6{\cdot}H_2O$ precursor after a fluorine-assisted hydrothermal route. With the increment of the reaction time, the morphology of precursor changed continually. In the formation process, sodium citrate plays a role of surfactant, and NH_4F serves as a source for the generation of both the ammonia cations and fluoride anion, as well as urea acts as the precipitant. The CNSs are interdigitated and perpendicular to the substrate, and the thickness of irregular nanosheets are 30–100 nm. The mesoporous structure can be obtained after annealing with the specific surface area of 83 $m^2\ g^{-1}$ and the average pore diameter of ~8.5 nm. Owing to the direct growth on the substrates, the Co_3O_4 CNS arrays could serve as a prototype gas sensor straightway. The sensor showed outstanding low temperature gas-sensing properties with a gas response of ~36.5 to 1000 ppm acetone vapour at 111 °C. The sensor also exhibited good selectivity and excellent stability.

1. Introduction

Until now, acetone as a volatile, flammable and deleterious compound has been widely used in the industrial application, especially in the fields of pharmaceuticals industry and pesticide preparation [1–3]. Additionally, acetone may threaten human's health with the concentration over 10,000 ppm, leading to headache, fatigue and even narcosis [4]. As the medical research reported, higher acetone concentration exists in exhaled breath of diabetic patients than healthy people [5]. Therefore, detecting acetone concentration in public or human body is urgent for confirming the safety and health. Recently, novel sensing materials have been largely developed to effectively monitor the acetone vapour. Previously, P. A. Murade et al. synthesized Sr-doped $LaFeO_3$ nanocrystalline-based gas sensors to detect acetone at 275 °C [6]. Gas sensors based on $SmFe_{1-x}Mg_xO_3$ were developed by Xing Liu et al. to analyze acetone vapour at 260 °C [4]. The operating temperature of porous $ZnFeO_4$ based gas sensors to detect the acetone reduces to 200 °C [7]. Nevertheless, low gas response and high operating temperature of the mentioned sensors directly result in the shorter lifetime and higher cost [8,9]. Thus, it is urgent to pursue novel materials to improve gas response at low operating temperature.

Cobalt oxide (Co_3O_4) with an intrinsic *p*-type property has been deeply studied in many technological fields, such as supercapacitors, heterogeneous catalysis, field-emission materials, lithium-ion battery electrodes, gas sensors and so on [10–19]. Developing novel Co_3O_4 nanostructures with specific sizes, well-defined features, and structures render a new approach to explore materials' physical and chemical properties [20–27]. Remarkable progress has been made in manufacturing a variety of Co_3O_4 nanomaterials with unique structures, such as hollow Co_3O_4 octahedral showing a good pseudocapacitance when being evaluated as an electrode material for supercapacitors [12], three dimensional Co_3O_4 dendrites with a low transition temperature of 35 K [28], star-like Co_3O_4 micro/nanostructures exhibiting high reversible capacity as an anode material in lithium ion batteries [29], and needlelike Co_3O_4 nanotubes with ultrahigh capacity with improved cycle life and high rate capability [30]. In recent years, various unique Co_3O_4 nanostructures for gas sensing with high gas response at low temperature have been synthesized, for example, the gas response of Co_3O_4 hollow nanotubes to 50 ppm formaldehyde attains 6.3 at 180 °C [31], the response of rhombus-shaped Co_3O_4 nanorod arrays toward 100 ppm ethanol vapour reaches 30 at 160 °C [32], and flower-like Co_3O_4 microspheres response to 100 ppm ethanol at 135 °C is 16 [33].

* Corresponding author.
E-mail address: zlp1@zju.edu.cn (L. Zhu).

http://dx.doi.org/10.1016/j.snb.2016.07.154
0925-4005/

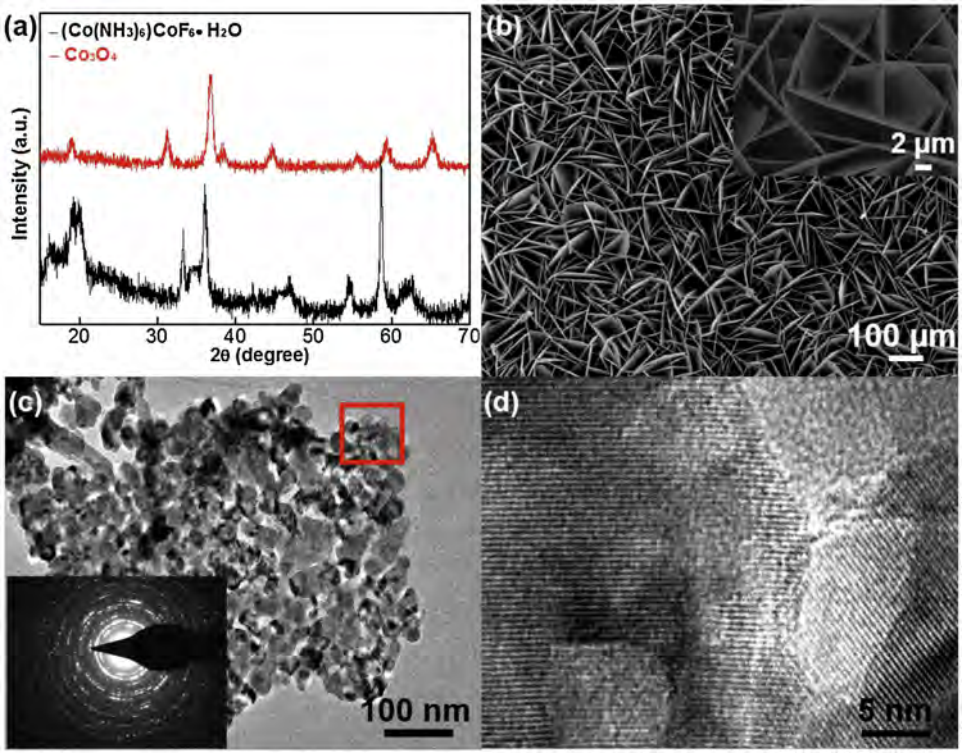

Fig. 1. (a) XRD patterns of as-prepared $(Co(NH_3)_6)CoF_6{\cdot}H_2O$ and Co_3O_4; (b) low magnified SEM images of Co_3O_4 crossed nanosheet arrays (inset is high magnified SEM image); (c) the TEM image of the individual nanosheet arrays (inset represents the SAED pattern); (d) HRTEM image taken from the area indicated by the red square in part c (for interpretation of the references to colour in this figure legend, the reader is referred to the web version of this article).

Herein, we have successfully synthesized Co_3O_4 CNS arrays by an approach of fluorine-assisted hydrothermal method followed by an annealing process. The growth mechanism of the CNS arrays was analyzed by studying the morphology of precursor with the increment of the reaction time. The as-obtained structures were characterized by several techniques, such as powder X-ray diffraction, scanning electron microscopies, transmission electron microscopy. The Co_3O_4 CNS arrays directly grow on the supporting substrates and intensively contact with the substrates, avoiding the conventional film formation process. The gas sensor based on Co_3O_4 crossed nanosheet arrays showed high gas response, great selectivity, excellent stability and large gas sensing response range at low operating temperature for acetone vapour.

2. Experimental

2.1. Synthesis

All chemicals were of analytical grade and used as purchased without further purification. Firstly, 8 mmol (0.48 g) urea ($CO(NH_2)_2$), 8 mmol (0.29 g) ammonium fluoride (NH_4F), 4 mmol (1.16 g) cobalt nitrate ($Co(NO_3)_2{\cdot}6H_2O$) and 0.03 mmol (0.01 g) sodium citrate ($C_6H_5Na_3O_7{\cdot}2H_2O$) were dissolved in 80 ml high purity water (18.2 MΩ cm resistivity), under stirring at room temperature until forming a pink homogeneous solution. Then, the solution was transferred into a 100 ml Teflon-lined stainless steel autoclave. A piece of cleaned polycrystalline alumina ceramics plate (13 mm × 7 mm, 0.5 mm in thick) which has been plated Ag-Pd interdigital electrodes, was immersed in the reaction solution. Afterwards, the autoclave was sealed and maintained at 95 °C for 12 h inside an electric oven. After cooling down to room temperature, the substrate was removed, rinsed with distilled water several times and dried at 70 °C for 2 h. Finally, after annealing at 350 °C in air atmosphere for 2 h, the as-prepared pink precursor converted to black Co_3O_4. The obtained prototype device can be directly used for gas sensing experiments.

2.2. Characterization

The crystal phase identification were investigated by XRD (Bede D1) system with Cu-Kα1 radiation (λ = 0.15406 nm) over the 2θ range of 10–70°. The microstructures and morphologies of Co_3O_4 CNS arrays were examined by SEM (Hitachi, S-4800) with an accelerating voltage of 5 kV. TEM and HRTEM images were taken by an HRTEM analyser (HRTEM, FEI F20) with an accelerating voltage of 200 kV. Thermogravimetric analysis (TGA) was carried out using a TA Q600 instrument in a temperature range from 25 °C to 500 °C with a heating rate of 10 °C/min in air. Specific surface areas were computed from the results of N_2 adsorption–desorption isotherms at 77 K (Micromeritics ASAP 3020). The electrical characteristics were measured at room temperature in the dark using a semiconductor parameter analyzer (Agilent E5270B) with the bias voltage range of −10–10 V.

2.3. Gas-sensing measurements

The detailed gas-sensing experimental process can be found in our previous report [34]. The gas sensing properties were measured by an intelligent gas sensing analysis system (CGS-1TP, Beijing Elite Tech Co., Ltd, China) as shown in Fig. S1. An external temperature control could adjust the temperature with a precision of 1 °C. Two probes were pressed onto the electrodes of sensor through adjusting the probe station. Before testing, the sensors were preheated at different operating temperatures for about 30 min to get the stable resistances. The target gas was injected into the test chamber (18 l in volume) through a rubber plug by a micro-injector. The target liquid, e.g. acetone, was injected into the evaporator inside to form acetone vapour. The saturated target gas was mixed with air (rela-

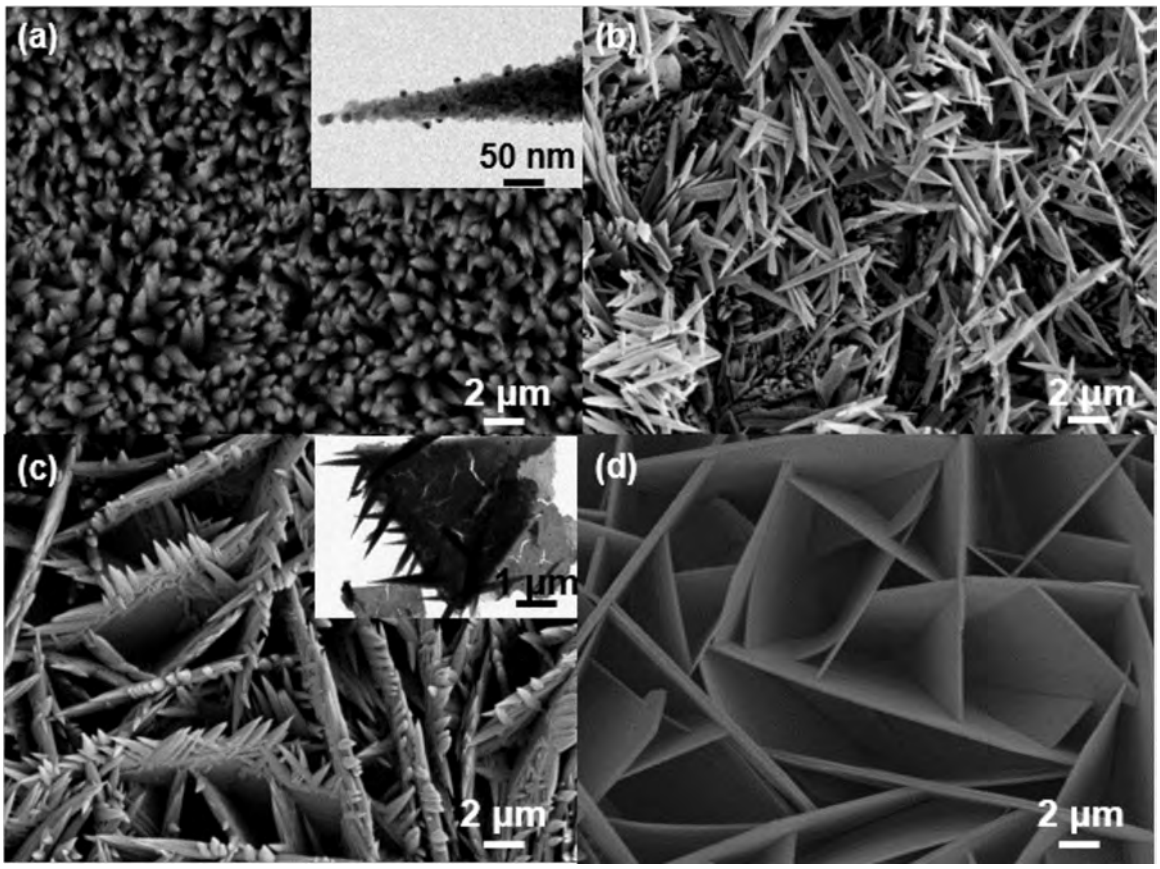

Fig. 2. SEM images of precursors with different growth time (a) 6 h, (b) 8 h, (c) 10 h and (d) 12 h, respectively. Insets in (a) and (c) are their corresponding TEM images.

tive humidity was 45% measured at 35 °C) by two fans inside. After the resistance reaching to a new constant value, the test chamber was opened to recover the sensor in air. The gas response was designated as R_g/R_a, where R_g is the sensor resistance measured in the presence of the target gas and R_a is in air. Response and recovery time were defined as the time needed for 90% of total resistance change on exposure to gas and air, respectively.

3. Results and discussion

The typical XRD patterns of the precursor and the calcined product are shown in Fig. 1a. The precursor pattern (black) is indexed as $(Co(NH_3)_6)CoF_6{\cdot}H_2O$. All of the diffraction peaks are in good agreement with the standard Joint Committee on Powder Diffraction Standards (JCPDS) card no. 24-0321. While the diffraction peaks of the product after calcination (red) are in good agreement with JCPDS card no. 43–1003 that indicate a cubic phase of Co_3O_4. Sharp and strong diffraction peaks confirm that the calcined product is pure in phase and well crystallized. No other peak of impurities was detected, revealing a complete thermal-conversion from $(Co(NH_3)_6)CoF_6{\cdot}H_2O$ to Co_3O_4. And the thermo-decomposition behavior of the precursor was studied by thermal-gravimetric (TG) analysis as shown in Fig. S2. Fig. 1b shows a low magnified SEM image of Co_3O_4 CNS arrays. It is obvious that large-scale and high density arrays of Co_3O_4 CNS are uniformly grown on the substrate. The inset of Fig. 1b shows a high magnified SEM image of the Co_3O_4 CNS arrays. We can see that the nanosheets are interdigitated and perpendicular to the substrate, and the thickness of irregular nanosheets are 30–100 nm. To further investigate crystallographic property, TEM and HRTEM characterizations were measured, and the corresponding images are shown in Fig. 1c and d, respectively The typical TEM image (Fig. 1c) reveals a single nanosheet, with a porous structure and rough surfaces, composed of many tiny single crystals with different growth orientations. The ring-like selected-area electron diffraction (SAED) pattern (inset of Fig. 1c) clearly verifies the Co_3O_4 nanosheet is polycrystalline in nature. The corresponding HRTEM image (Fig. 1d) taken from the area marked with a red square in Fig. 1c further proves the polycrystalline structure.

In order to understand the evolution process of the Co_3O_4 CNS arrays, a series of time-dependent experiments was carried out. The products obtained at different reaction time were characterized by SEM. No product was obtained when the reaction time was less than 6 h, which is due to the coordination of sodium citrate [35,36]. The representative SEM images of the products shown in Fig. 2 were acquired stepwise after 6, 8, 10 and 12 h of reaction. After 6 h of reaction, orderly nanoneedle arrays vertical to the substrate formed (Fig. 2a). When the reaction time increased to 8 h (Fig. 2b), another layer of nanoneedles with different orientation appeared on the top of as-prepared nanoneedles arrays. After another 2 h (Fig. 2c and inset), it can be inferred that the product was the combination of nanoneedles and nanosheets. In addition, these nanosheets are interdigitated, in other words, the nanosheets derive from the mutually perpendicular cross nanoneedles in one plane. Furthermore, when the reaction time extended to 12 h, the stable CNS arrays were successfully synthesized (Fig. 2d).

A schematic representation of the morphological evolution process of the CNS arrays is presented in Fig. 3. Firstly, the orderly nanoneedle arrays vertical to the substrate were formed. Then, a new layer of mussy nanoneedles appeared on the top of as-prepared nanoneedles arrays. Afterwards, the as-prepared arrays

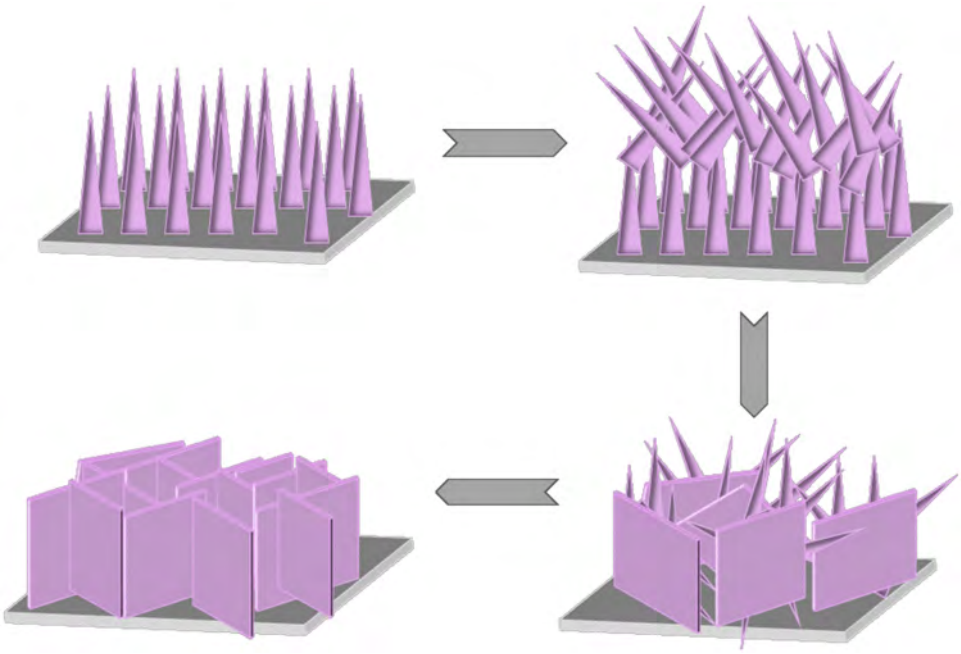

Fig. 3. Schematic diagram of the fabricating process.

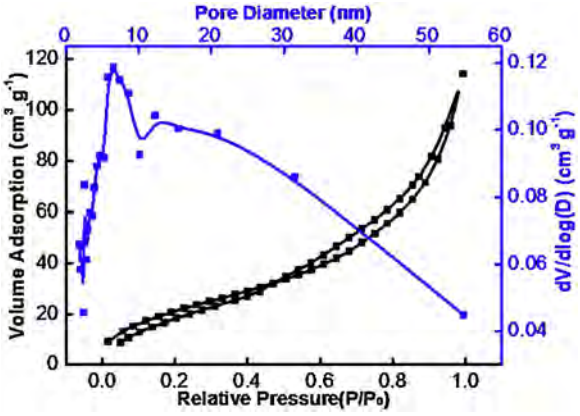

Fig. 4. Nitrogen adsorption-desorption isotherms and pore size distribution curves for the Co_3O_4 crossed nanosheet arrays.

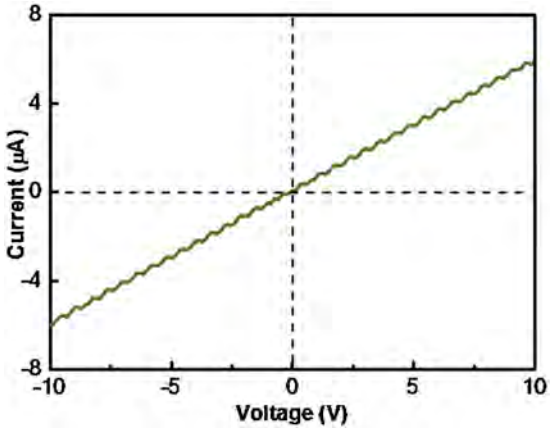

Fig. 5. *I–V* characteristics between the two neighboring electrodes, bridged by the Co_3O_4 crossed nanosheet arrays.

gradually became the combination of nanoneedles and nanosheets. Ultimately, stable and high density CNS arrays are uniformly grown on the substrate. The formation of the CNS arrays is attributed to the minimization of surface energy and subsequent Ostwald ripening, in which the initial nanoneedles dissolve and regrow into the special crossed nanosheet arrays [29,37,38]. In this experiment, sodium citrate is surfactant [39,40], NH_4F in these reactions served mainly as a source for the generation of both the ammonia cations and fluoride anion [41], and urea played the role of precipitant. In addition, when the solution contains sufficient amount of urea, it's highly possible to form a two-layer structure [42–44].

N_2 sorption measurements were evaluated for characterizing the porous properties of Co_3O_4 CNS arrays and gathering information about the specific surface area and pore size distribution. Fig. 4 displays the nitrogen adsorption-desorption isotherms and pore size distribution curves for the Co_3O_4 CNS arrays, both of which reveal a typical type IV adsorption isotherm with a H3-type hysteresis loop at different relative pressure ranges. The Co_3O_4 CNS arrays has a BET surface area of 83 $m^2\ g^{-1}$ with an average BJH pore diameter of 8.5 nm, indicating the presence of mesoporous (2–50 nm) [43]. In fact, the mesoporosity could be reasonably deduced from the pyrolysis and release of HF, NH_3 and H_2O during the thermal conversion [45].

Due to the large surface area and mesoporous structure revealed in the Co_3O_4 CNS arrays, it is worthwhile to study their gas-sensing performance. The Co_3O_4 CNS arrays vertically grew on the ceramic substrate, which could serve as a prototype sensor. Fig. 5 plots a typical current–voltage (*I–V*) characteristics of an as-fabricated gas sensor. The Co_3O_4 nanosheets vertically grew on the substrate and intersected with each other, forming ordered crossed nanosheet arrays with a highly open and porous structure. The resultant structure provides the high-speed electrical channels between the neighboring electrodes [46]. Linearly increased current with applied bias of *I–V* curves reveals good ohmic contact between the crossed Co_3O_4 arrays and the electrodes, ensuring that all upcoming behaviors of electrical devices represent the gas-sensing properties but not the contact between the material and the electrodes [32,47].

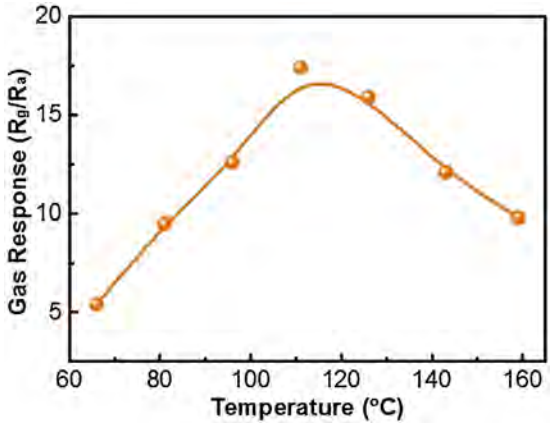

Fig. 6. Responses of Co_3O_4 nanosheet arrays to 100 ppm acetone at different operating temperatures.

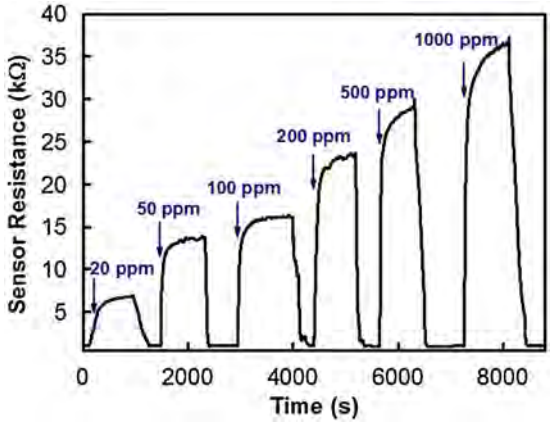

Fig. 7. The representative response and recovery curve of the Co_3O_4 crossed nanonsheets arrays gas sensor to acetone with concentrations ranging from 20 to 1000 ppm at 111 °C.

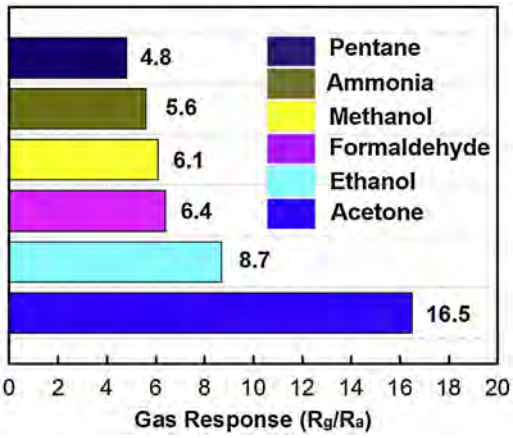

Fig. 8. Comparison of the gas response of Co_3O_4 crossed nanosheet arrays to various gases with 100 ppm concentration at 111 °C.

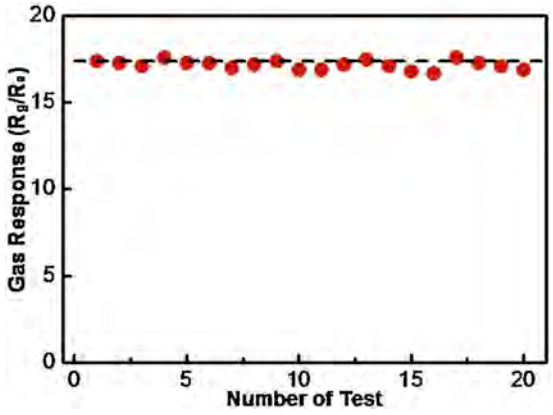

Fig. 9. Responses to 100 ppm acetone (RH = 45% measured at 35 °C) repeated with 20 times test during two months at 111 °C.

The gas sensing properties of the Co_3O_4 CNS arrays were studied with acetone as probe gas. It is well known that the operating temperature has great influence on sensing properties, especially the gas response [48–51]. There is usually a temperature region where the sensor shows the highest gas response. A Co_3O_4 CNS arrays based gas sensor was exposed to 100 ppm of acetone at different operating temperatures. The sensor response as a function of operating temperature from 60 °C to 160 °C is plotted in Fig. 6. The gas responses increased until reaching the maximum at 111 °C, and then decreased rapidly with further increasing of operating temperature. The gas adsorption and desorption kinetics on the surface of sensing materials can be used to explain this behavior [9,40,52]. When the operating temperature is relatively low, the chemical activation of Co_3O_4 nanosheets are consequently low, leading to a low response. But if the operating temperature is too high, some adsorbed gas molecules may escape from the surface of sensing materials before reaction, thus gas response decreases correspondingly.

Fig. 7 displays the dynamic response–recovery curves of the Co_3O_4 CNS arrays based sensor toward different acetone concentrations ranging from 20 to 1000 ppm. The gas response increases rapidly with increasing concentration of acetone in this range, that toward 20, 50, 100, 200, 500 and 1000 ppm of acetone are 6.8, 13.6, 16.5, 23.4, 29 and 36.5, respectively. The result indicates that the sensor could detect acetone gas in a wide range of concentrations, which is the indispensable requirement of sensors to meet the needs of various environment. The special structure of Co_3O_4 CNS arrays may be the major factor leading to the increase of gas response. Generally, compared with the unordered structure, the long-range structure can lower the internal resistance, facilitating the electron transfer rate [53]. In addition, the nanoarray architecture not only prevents agglomeration but also provides large surface area and more active sites to absorb O_2, and the open space among the neighboring nanosheets allows fast absorption and desorption reactions [54].

Another important parameter of sensor property is selectivity. Fig. 8 presents the acetone-selective characteristics of Co_3O_4 CNS arrays with respect to other typical interfering gases such as ethanol, formaldehyde, ammonium, methanol and pentane at 111 °C. The gas response to 100 ppm acetone is 16.5, which is significantly higher than all the other gases on the same concentration. The response to ethanol, formaldehyde, methanol, ammonia and pentane is as low as 8.7, 6.4, 6.1, 5.6 and 4.8, respectively. It is obviously that the gas sensors based on Co_3O_4 CNS arrays exhibit good selectivity toward acetone.

To confirm the repeatability of sensors, the response of the Co_3O_4 CNS arrays-based sensors to 100 ppm acetone repeated with 20 times test during two months. The result shown in Fig. 9 illustrates that there is almost no apparent signal attenuation during the long-term test. Therefore, it is concluded that the stability of the sensors is good enough to detect acetone vapour in a long time.

The gas sensing mechanism for Co_3O_4 CNS arrays consists of the change in electrical conductivity on account of the chemical interaction of gas molecules with the surface involving gas adsorption, surface reaction, and desorption processes as we discussed in the

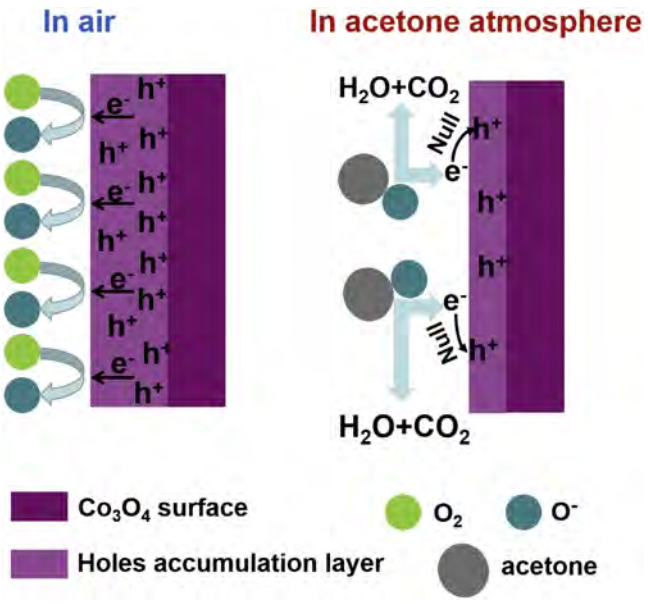

Fig. 10. Schematic diagram of the gas sensing mechanism.

previous articles [15,34]. Fig. 10 illustrates the schematic diagram of the acetone gas sensing mechanism. Co_3O_4 is a *p*-type semiconductor thus holes are the main charge carrier. When exposed to air, O_2 adsorption on the Co_3O_4 surface traps electrons from the conduction band of the semiconductor to form oxygen species (O_2^-, O^{2-}, or O^-), and form the depletion layer with a consequent low resistance of the sensor. Once the sensor exposed to acetone gas, the acetone molecules react with the adsorbed oxygen ions, then the captured electrons released, thus, the charge carrier accumulation layer near the surface is thinned by the electrochemical interaction between O^- and gas molecules, as in the following Reaction (1), which releases free electrons and neutralizes the holes in the Co_3O_4 (2), leading to the increase of the baseline resistivity until a dynamic equilibrium condition is obtained:

$$CH_3COCH_3(gas) + 8O^- \rightarrow 3CO_2 + 3H_2O + 8e^- \quad (1)$$

$$e^- + h^+ \rightarrow Null \quad (2)$$

What's more, the sensors based on orderly vertically arrays can offer more active area to absorb oxygen and promote the diffusion rate of probe gas to enhance sensing properties. When stopping the acetone flow, oxygen molecules in the air are absorbed on the surface of the sensors again, thus the resistance decreases to its initial value.

The high performance for acetone detection can be attributed to the unique structure of Co_3O_4 CNS arrays. Firstly, the direct growth of Co_3O_4 CNS on the substrate promotes each nanosheet to participate in the gas sensing reaction [55]. Good ohmic contact between the electrodes and Co_3O_4 CNS arrays make it possible to use Co_3O_4 CNS arrays directly as gas sensors without the conventional film formation process. Secondly, the Co_3O_4 nanosheets are polycrystalline, which consists of many small grains. Gas molecules can be stored in the interface and boundary of grains, thus enhancing the gas response [56]. Additionally, the high crystallinity of the Co_3O_4 nanosheets dramatically increases the long-term stability of the sensors [57]. Thirdly, The Co_3O_4 nanosheets vertically grow on the substrate and intersect with each other, forming ordered CNS arrays with a highly open structure. The resultant structure not only provides prevents agglomeration but also provides the high-speed electrical channels between the neighboring electrodes [54]. Fourthly, the high surface-to-volume ratio of CNS arrays can supply more active reaction sites for adsorption, transportation and desorption of gas molecules. Moreover, the mesoporous structures allow the gas molecules to easily penetrate and adsorb on the surface leading to high gas response [58].

4. Conclusions

In summary, a kind of Co_3O_4 crossed nanosheet arrays were successfully synthesized via a facile fluorine-assisted hydrothermal method. The growth mechanism has been comprehended by studying the morphology of precursor with the increment of the reaction time. In the formation process, sodium citrate plays a role of surfactant, NH_4F serves as a source for the generation of both the ammonia cations and fluoride anion, and urea acts as the precipitant. The CNSs, with the thickness of 30–100 nm, the specific surface area of 83 $m^2\ g^{-1}$ and a pore diameter of ~8.5 nm, are interdigitated and perpendicular to the substrate. Due to the good Ohmic contact with the electrodes, and intensive contact with the substrate and Co_3O_4 CNS arrays, the Co_3O_4 CNS arrays could directly serve as gas sensors without the conventional film formation process. This highly open and porous structure not only prevents agglomeration but also leads to more active sites to absorb O_2, and the open space among the neighboring nanosheets allows fast absorption and desorption reactions. The gas sensors based Co_3O_4 CNS arrays show great performance for detecting acetone, the response to 1000 ppm acetone reached ~36.5 with its optimal working temperature as low as 111 °C. What's more, sensors can detect acetone in a wide range of concentrations starting with a low detection limit and exhibit good reproducibility and stability. The high-performance results from the unique structure of crossed nanosheet arrays with a variety of excellent features, mesoporous structure and large specific surface. The fabrication of the high-performance gas sensors possesses the capability of constructing complex architectures with the Co_3O_4 CNS arrays as the building block.

Acknowledgements

This work was supported by National Natural Science Foundation of China (51372224, 51572239), Program for Innovative Research Team in University of Ministry of Education of China (IRT13037) and Cyrus Tang fund for Sensor Materials and Applications.

Appendix A. Supplementary data

Supplementary data associated with this article can be found, in the online version, at http://dx.doi.org/10.1016/j.snb.2016.07.154.

References

[1] S.A. El-Gizawy, M.A. Osman, M.F. Arafa, G.M. El Maghraby, Aerosil as a novel co-crystal co-former for improving the dissolution rate of hydrochlorothiazide, Int. J. Pharm. 478 (2015) 773–778.
[2] C. Huang, X.Y. Yang, L. Xiong, H.J. Guo, J. Luo, B. Wang, et al., Evaluating the possibility of using acetone-butanol-ethanol (ABE) fermentation wastewater for bacterial cellulose production by Gluconacetobacter xylinus, Lett. Appl. Microbiol. 60 (2015) 491–496.
[3] Y. Sapozhnikova, T. Simons, S.J. Lehotay, Evaluation of a fast and simple sample preparation method for polybrominated diphenyl ether (PBDE) flame retardants and dichlorodiphenyltrichloroethane (DDT) pesticides in fish for analysis by ELISA compared with GC–MS/MS, J. Agric. Food Chem. 63 (2015) 4429–4434.
[4] X. Liu, J. Hu, B. Cheng, H. Qin, M. Jiang, Acetone gas sensing properties of $SmFe_{1-x}MgxO_3$ perovskite oxides, Sens. Actuators B: Chem. 134 (2008) 483–487.
[5] M. Righettoni, A. Tricoli, Toward portable breath acetone analysis for diabetes detection, J. Breath Res. 5 (2011) 037109.
[6] P.A. Murade, V.S. Sangawar, G.N. Chaudhari, V.D. Kapse, A.U. Bajpeyee, Acetone gas-sensing performance of Sr-doped nanostructured $LaFeO_3$ semiconductor prepared by citrate sol–gel route, Curr. Appl. Phys. 11 (2011) 451–456.

[7] X. Zhou, J. Liu, C. Wang, P. Sun, X. Hu, X. Li, et al., Highly sensitive acetone gas sensor based on porous $ZnFe_2O_4$ nanospheres, Sens. Actuators B: Chem. 206 (2015) 577–5783.
[8] N. Yamazoe, K. Shimanoe, New perspectives of gas sensor technology, Sens. Actuators B: Chem. 138 (2009) 100–107.
[9] M. Gardon, J.M. Guilemany, A review on fabrication, sensing mechanisms and performance of metal oxide gas sensors, J. Mater. Sci. Mater. Electron. 24 (2012) 1410–1421.
[10] N. Rezlescu, N. Iftimie, E. Rezlescu, C. Doroftei, P.D. Popa, Semiconducting gas sensor for acetone based on the fine grained nickel ferrite, Sens. Actuators B: Chem. 114 (2006) 427–432.
[11] B. Varghese, C.H. Teo, Y. Zhu, M.V. Reddy, B.V.R. Chowdari, A.T.S. Wee, et al., Co_3O_4 nanostructures with different morphologies and their field-emission properties, Adv. Funct. Mater. 17 (2007) 1932–1939.
[12] Y. Cao, F. Yuan, M. Yao, J.H. Bang, J.-H. Lee, A new synthetic route to hollow Co_3O_4 octahedra for supercapacitor applications, CrystEngComm 16 (2014) 826–833.
[13] Y. Teng, L.X. Song, L.B. Wang, J. Xia, Face-raised octahedral Co_3O_4 nanocrystals and their catalytic activity in the selective oxidation of alcohols, J. Phys. Chem. C 118 (2014) 4767–4773.
[14] W. Mei, J. Huang, L. Zhu, Z. Ye, Y. Mai, J. Tu, Synthesis of porous rhombus-shaped Co_3O_4 nanorod arrays grown directly on a nickel substrate with high electrochemical performance, J. Mater. Chem. 22 (2012) 9315–9321.
[15] Z. Zhang, Z. Wen, Z. Ye, L. Zhu, Gas sensors based on ultrathin porous Co_3O_4 nanosheets to detect acetone at low temperature, RSC Adv. 5 (2015) 59976–59982.
[16] Z. Wen, J. Chen, M.-H. Yeh, H. Guo, Z. Li, X. Fan, et al., Blow-driven triboelectric nanogenerator as an active alcohol breath analyzer, Nano Energy 16 (2015) 38–46.
[17] Y. Liu, G. Zhu, B. Ge, H. Zhou, A. Yuan, X. Shen, Concave Co_3O_4 octahedral mesocrystal: polymer-mediated synthesis and sensing properties, CrystEngComm 14 (2012) 62–64.
[18] J.Y. Kim, N.-J. Choi, H.J. Park, J. Kim, D.-S. Lee, H. Song, A hollow assembly and its three-dimensional network formation of single-crystalline Co_3O_4 nanoparticles for ultrasensitive formaldehyde gas sensors, J. Phys. Chem. C 118 (2014) 25994–26002.
[19] Y. Liu, G. Zhu, J. Chen, H. Xu, X. Shen, A. Yuan, Co_3O_4/ZnO nanocomposites for gas-sensing applications, Appl. Surf. Sci. 265 (2013) 379–384.
[20] X.W.D. Lou, L.A. Archer, Z. Yang, Hollow micro-nanostructures synthesis and applications, Adv. Mater. 20 (2008) 3987–4019.
[21] N. Pinna, M. Niederberger, Surfactant-free nonaqueous synthesis of metal oxide nanostructures, Angew. Chem. 47 (2008) 5292–52304.
[22] X.-G. Han, H.-Z. He, Q. Kuang, X. Zhou, X.-H. Zhang, Tao Xu, et al., Controlling morphologies and tuning the related properties of NanoMicrostructured ZnO crystallites, J. Phys. Chem. C 113 (2009) 584–589.
[23] D. Su, H. Fu, X. Jiang, G. Wang, ZnO nanocrystals with a high percentage of exposed reactive facets for enhanced gas sensing performance, Sens. Actuators B: Chem. 186 (2013) 286–292.
[24] L. Wang, J. Deng, Z. Lou, T. Zhang, Nanoparticles-assembled Co_3O_4 nanorods p-type nanomaterials: one-pot synthesis and toluene-sensing properties, Sens. Actuators B: Chem. 201 (2014) 1–6.
[25] J. Deng, L. Wang, Z. Lou, T. Zhang, Fast response/recovery performance of comb-like Co_3O_4 nanostructure, RSC Adv. 4 (2014) 211–215.
[26] H.J. Park, N.-J. Choi, H. Kang, M.Y. Jung, J.W. Park, K.H. Park, et al., A ppb-level formaldehyde gas sensor based on CuO nanocubes prepared using a polyol process, Sens. Actuators B: Chem. 203 (2014) 282–288.
[27] H.J. Park, J. Kim, N.J. Choi, H. Song, D.S. Lee, Nonstoichiometric Co-rich $ZnCo_2O_4$ hollow nanospheres for high performance formaldehyde detection at ppb levels, ACS Appl. Mater. Interfaces 8 (2016) 3233–3240.
[28] L. Zhang, X. Zhao, W. Ma, M. Wu, N. Qian, W. Lu, Novel three-dimensional Co_3O_4 dendritic superstructures: hydrothermal synthesis, formation mechanism and magnetic properties, CrystEngComm 15 (2013) 1389–1396.
[29] L. Li, K.H. Seng, Z. Chen, Z. Guo, H.K. Liu, Self-assembly of hierarchical star-like Co_3O_4 micro/nanostructures and their application in lithium ion batteries, Nanoscale 5 (2013) 1922–1928.
[30] X.W. Lou, D. Deng, J.Y. Lee, J. Feng, L.A. Archer, Self-supported formation of needlelike Co_3O_4 nanotubes and their application as lithium-ion battery electrodes, Adv. Mater. 20 (2008) 258–262.
[31] S. Wang, C. Xiao, P. Wang, Z. Li, B. Xiao, R. Zhao, et al., Co_3O_4 hollow nanotubes: facile synthesis and gas sensing properties, Mater. Lett. 137 (2014) 289–292.
[32] Z. Wen, L. Zhu, W. Mei, Y. Li, L. Hu, L. Sun, et al., A facile fluorine-mediated hydrothermal route to controlled synthesis of rhombus-shaped Co_3O_4 nanorod arrays and their application in gas sensing, J. Mater. Chem. A 1 (2013) 7511–7518.
[33] C. Sun, S. Rajasekhara, Y. Chen, J.B. Goodenough, Facile synthesis of monodisperse porous Co_3O_4 microspheres with superior ethanol sensing properties, Chem. Commun. 47 (2011) 12852–12854.
[34] Z. Wen, L. Zhu, W. Mei, L. Hu, Y. Li, L. Sun, et al., Rhombus-shaped Co_3O_4 nanorod arrays for high-performance gas sensor, Sens. Actuators B: Chem. 186 (2013) 172–179.
[35] H. Du, L. Jiao, Q. Wang, J. Yang, L. Guo, Y. Si, et al., Facile carbonaceous microsphere templated synthesis of Co_3O_4 hollow spheres and their electrochemical performance in supercapacitors, Nano Res. 6 (2012) 87–98.
[36] S. Mehrizi, M.H. Sohi, M. Saremi, Effect of sodium citrate as complexing on electrochemical behavior and speciation diagrams of CoFeNiCu baths, Ionics 19 (2012) 911–918.
[37] Y.-B. Cao, X. Zhang, J.-M. Fan, P. Hu, L.-Y. Bai, H.-B. Zhang, et al., Synthesis of hierarchical Co micro/nanocomposites with hexagonal plate and polyhedron shapes and their catalytic activities in glycerol hydrogenolysis, Cryst. Growth Des. 11 (2011) 472–479.
[38] A. Rothschild, The effect of grain size on the sensitivity of nanocrystalline metal-oxide gas sensors, J. Appl. Phys. 95 (2004) 63–74.
[39] R.-T. Wang, L.-B. Kong, J.-W. Lang, X.-W. Wang, S.-Q. Fan, Y.-C. Luo, et al., Mesoporous Co_3O_4 materials obtained from cobalt–citrate complex and their high capacitance behavior, J. Power Sources 217 (2012) 358–363.
[40] F. Yang, Z. Guo, Comparison of the enhanced gas sensing properties of tin dioxide samples doped with different catalytic transition elements, J. Colloid. Interf. Sci. 448 (2015) 265–274.
[41] R.X. Chen, S.L. Zhu, J. Mao, Z.D. Cui, X.J. Yang, Y.Q. Liang, et al., Synthesis of CuO/Co_3O_4 coaxial heterostructures for efficient and recycling photodegradation, Int. J. Photoenergy 2015 (2015) 1–11.
[42] Z.H. Ibupoto, S. Elhag, M.S. AlSalhi, O. Nur, M. Willander, Effect of urea on the morphology of Co_3O_4 nanostructures and their application for potentiometric glucose biosensor, Electroanalysis 26 (2014) 1773–1781.
[43] S. Xiong, J.S. Chen, X.W. Lou, H.C. Zeng, Mesoporous Co_3O_4 and CoO@C topotactically transformed from chrysanthemum-like $Co(CO_3)_{0.5}(OH)\cdot 0.11H_2O$ and their lithium-Storage properties, Adv. Funct. Mater. 22 (2012) 861–871.
[44] Y. Yao, J. Zhang, T. Huang, H. Mao, A. Yu, Porous Co_3O_4 nanoflakes as anode material for lithium ion batteries, Int. J. Electrochem. Sci. 8 (2013) 3302–3309.
[45] X. Xia, J. Tu, Y. Mai, X. Wang, C. Gu, X. Zhao, Self-supported hydrothermal synthesized hollow Co_3O_4 nanowire arrays with high supercapacitor capacitance, J. Mater. Chem. 21 (2011), 93–19.
[46] Q. Yang, Z. Lu, X. Sun, J. Liu, Ultrathin Co_3O_4 nanosheet arrays with high supercapacitive performance, Sci. Rep. 3 (2013) 35–37.
[47] K. Subramanyam, N. Sreelekha, D. Amaranatha Reddy, G. Murali, R.P. Vijayalakshmi, Influence of Co co-doping on structural, optical and magnetic properties of SnO_2:Cr nanoparticles, Superlattices Microstruct. 82 (2015) 207–218.
[48] W.X. Jin, S.Y. Ma, Z.Z. Tie, J.J. Wei, J. Luo, X.H. Jiang, et al., One-step synthesis and highly gas-sensing properties of hierarchical Cu-doped SnO_2 nanoflowers, Sens. Actuators B: Chem. 213 (2015) 171–180.
[49] L. Zhang, Z. Gao, C. Liu, Y. Zhang, Z. Tu, X. Yang, et al., Synthesis of TiO_2 decorated Co_3O_4 acicular nanowire arrays and their application as an ethanol sensor, J. Mater. Chem. A 3 (2015) 2794–2801.
[50] J. Deng, B. Yu, Z. Lou, L. Wang, R. Wang, T. Zhang, Facile synthesis and enhanced ethanol sensing properties of the brush-like ZnO–TiO_2 heterojunctions nanofibers, Sens. Actuators B Chem. 184 (2013) 21–26.
[51] J. Deng, L. Wang, Z. Lou, T. Zhang, Design of CuO–TiO_2 heterostructure nanofibers and their sensing performance, J. Mater. Chem. A 2 (2014) 9030–9034.
[52] H. Kim, J. Lee, Highly sensitive and selective gas sensors using p-type oxide semiconductors: overview, Sens. Actuators B: Chem. 192 (2014) 607–627.
[53] Y. Hsu, Y. Chen, Y. Lin, L. Chen, K. Chen, Reversible phase transformation of MnO_2 nanosheets in an electrochemical capacitor investigated by in situ Raman spectroscopy, Chem. Comm. 47 (2011) 1252–1254.
[54] Y. Li, B. Tan, Y. Wu, Mesoporous Co_3O_4 nanowire arrays for lithium ion batteries with high capacity and rate capability, Nano Lett. 8 (2007) 265–270.
[55] K. Choi, H. Kim, K. Kim, D. Liu, G. Cao, J. Lee, C_2H_5OH sensing characteristics of various Co_3O_4 nanostructures prepared by solvothermal reaction, Sens. Actuators B: Chem. 146 (2010) 183–189.
[56] N.L. Hung, H. Kim, S. Hong, D. Kim, A simple fabrication method of randomly oriented polycrystalline zinc oxide nanowires and their application to gas sensing, Adv. Nat. Sci.: Nanosci. Nanotechnol. 2 (2011) 015002.
[57] H. Nguyen, S.A. El-Safty, Meso- and macroporous Co_3O_4 nanorods for effective VOC gas, J. Phys. Chem. C 115 (2011) 8466–88474.
[58] Y. Cui, Q. Wei, H. Park, C.M. Lieber, Nanowire nanosensors for highly sensitive and selective detection of biological and chemical species, Science 293 (2001) 1289–1292.

Biographies

Ziyue Zhang received BS degree at Northwestern Polytechnical University in 2013. She is currently pursuing Ph.D degree at Zhejiang University. Her current fields of interests include design and synthesis of nano-materials and study their gas sensing properties.

Liping Zhu received her BSc (1988) and MSc (1991) degrees in Materials Science from Zhejiang University. She studied in Hiroshima University in Japan as a doctoral student from 1998 to 2002. Then she joined the Materials Department of Zhejiang University since 2002. Her current research interests include semiconductor materials, photo-electronic thin films, nano-materials and their application in devices.

Zhen Wen received his B.S. degree in Materials Science and Engineering from China University of Mining and Technology (CUMT) in 2011. He started to pursue his Ph.D. degree at Zhejiang University (ZJU) after that. Now he is a Ph.D. candidate in Materials Science and Engineering at Zhejiang University. His research interests mainly focus on nanomaterials and nano energy.

Zhizhen Ye received his B.S. degree in Electrical Engineering, received his M.S. degree and his Ph.D. in Optical Engineering from Zhejiang University in 1981, 1984 and 1987 respectively. He has been a professor of materials science and engineering since 1994. His research interests are in the area of heterogrowth and devices fabrication of silicon-based thin films.